European Cells and Materials Vol. 40 2020 (pages 133-145) DOI: 10.22203/eCM.v040a08 ISSN 1473-2262

INCREASED VASCULOGENESIS OF ENDOTHELIAL CELLS IN HYALURONIC ACID AUGMENTED FIBRIN-BASED NATURAL HYDROGELS – FROM *IN VITRO* TO *IN VIVO* MODELS

H.C. Lin[1,2], C.K. Wang[3], Y.C. Tung[1,4], F.Y. Chiu[2,5] and Y.P. Su[2,5,*]

[1] Research Centre for Applied Sciences, Academia Sinica, Taipei 11529, Taiwan
[2] Department of Orthopaedics and Traumatology, Taipei Veterans General Hospital, Taipei 11217, Taiwan
[3] Department of Mechanical Engineering, National Taiwan University, Taipei, 10617, Taiwan
[4] College of Engineering, Chang Gung University, Taoyuan 33302, Taiwan
[5] Department of Medicine, National Yang-Ming University, Taipei 11221, Taiwan

Abstract

Vascularisation efficiency plays an essential role in the success of bulk transplantation, while biocompatibility and safety are major concerns in clinical applications. Fibrin-based hydrogels have been exploited as scaffolds for their advantages in biocompatibility, degradability and mass transportation in various forms. However, the mechanical strength and degree of vascularisation remain unsatisfactory for clinical usage. An interpenetrating hydrogel was developed by adding hyaluronic acid (HA) to a fibrin-based natural hydrogel. The vasculogenesis of endothelial cells (human umbilical vein endothelial cells, HUVECs) was characterised within the gel using both *in vitro* and *in vivo* animal studies. The *in vitro* vascular morphology analysis showed 17.9 % longer mean tube length and 14.3 % higher average thickness in 7 d cultivation within the HA-supplemented hydrogel. The *in vivo* results showed 51.6 % larger total tube area, 1.8 × longer average tube length and 81.6 % higher cell number in the HA-supplemented hydrogel compared to the hydrogel without HA. The experimental results demonstrated better vascularisation and cell recruitment in the HA- supplemented hydrogel. The material properties of the hydrogels were also analysed using atomic force microscopy (AFM). The results revealed 3.7 × higher elasticity of the HA-supplemented hydrogel, which provided better mechanical strength and support for easy handling during procedures. With the demonstrated advantages, the developed hydrogels showed promise for exploitation in various practical clinical applications.

Keywords: Hydrogel, hyaluronic acid, fibrin gel, vasculogenesis, endothelial cell.

***Address for correspondence**: Yu-Ping Su, Department of Orthopaedics and Traumatology, Taipei Veterans General Hospital, 201, Sec. 2, Shih-Pai Road, Taipei 112, Taiwan.
Telephone number: +886-2-28757557…Fax number: +886-2-28757657…Email: ericypsu@gmail.com

Introduction

Tissue and organ transplantations have been exploited as ultimate solutions for various diseases and pathological conditions in clinical procedures (Brown and Cruess, 1982; Curl *et al.*, 1997). Bulk transplants often give sub-optimal results due to their inadequate vascularisation (Pelissier *et al.*, 2003). For example, lack of blood supply is one of the critical causes for fracture non-union and poor healing of tendon repair in orthopaedic surgeries (Kimball *et al.*, 2007; Richards, 1980). To improve the vascularisation, establishing a well-penetrated pre-vascularisation endothelium network *in vitro*, before implantation, has been investigated (Laschke and Menger, 2016; Novosel *et al.*, 2011). The primitive vasculature allows for rapid integration with the host circulation and supports maturation of the vessels, thus increasing the implant perfusion and survival (Gibot *et al.*, 2010; Levenberg *et al.*, 2005; Tremblay *et al.*, 2005). However, it is challenging to engineer an *in vitro* vasculature for clinical applications because of the relatively low process efficiency and concerns over compatibility and safety (Laschke and Menger, 2016).

In order to promote vascularisation, hydrogels have been widely studied as potential scaffolds because of their advantages in biocompatibility, degradability, mass transportation and injectability

as well as provision of an aqueous environment (Hoffman, 2012; Khademhosseini and Langer, 2007). Fibrin gel, a natural hydrogel, is a well-established material for studying vascularisation. As the primary matrix in wound healing, the three-dimensional (3D) structure of fibrin provides a solid scaffold for haemostasis (Laurens *et al.*, 2006). Fibrin gels with added angiogenic growth factors can stimulate endothelial cell growth for several days by slowly releasing angiogenic factors (Wong *et al.*, 2003). Therefore, fibrin gel is suitable for long-term differential culture due to its desirable properties. Furthermore, fibrin promotes production of extracellular matrix (ECM) proteins (*e.g.* collagen I). This provides stable microvascular networks and adhesion sites for the endothelial cells as well as regulating endothelial cell migration, proliferation and survival (Grassl *et al.*, 2002; Morin and Tranquillo, 2013; Raines, 2000). However, fibrin gel containing cells usually contracts and degrades rapidly during *in vitro* culture and transplantation (Lorentz *et al.*, 2011; Meinhart *et al.*, 1999; Park *et al.*, 2009; Rowe and Stegemann, 2006; Syedain *et al.*, 2009; Tuan *et al.*, 1996). This poor mechanical property of fibrin gel is a disadvantage for practical applications. To improve the properties of the fibrin gel, hydrogels made of fibrin with other materials – forming interpenetrating polymer network (IPN) hydrogels – have been investigated to overcome the drawbacks. IPN is a polymer which comprises two or more networks that are, at least, partially interlaced on a polymer scale but not covalently bonded to each other. It has been shown that the networks can be stably maintained without separation for various applications (McNaught and McNaught, 1997).

Among various synthetic or natural materials forming an IPN hydrogel with fibrin is hyaluronic acid (HA), a native component of extracellular matrix, which has been exploited to form networks with fibrin. The fibrin and HA are crosslinked to form an IPN structure and the scaffold formed can maintain its integrity for more than 2 weeks (Yu *et al.*, 2015). HA is a glycosaminoglycan that distributes ubiquitously in connective tissues to support the matrices. Previous studies have reported that HA concentrations elevate at inflammation sites and in damaged tissues immediately after the formation of fibrin gels (LeBoeuf *et al.*, 1986; Weigel *et al.*, 1986). HA can specifically bind to fibrinogen and improve the polymerisation process, stabilise the fibrin gel and delay the degradation (Komorowicz *et al.*, 2017; LeBoeuf *et al.*, 1987; LeBoeuf *et al.*, 1986). By modulating the architecture, large HA molecules can also increase the porosity of fibrin gel and largely stimulate cell migration within the 3D construct (Hayen *et al.*, 1999; Komorowicz *et al.*, 2017). High molecular weight HA, usually defined as that with a molecular mass greater than 1×10^6 Da, is anti-angiogenic because it promotes cell quiescence and tissue integrity (Genasetti *et al.*, 2008; Maharjan *et al.*, 2011; Rooney *et al.*, 1995). In contrast, the low molecular weight HA ($0.8\text{-}8 \times 10^5$ Da) or oligo-HA ($< 6 \times 10^3$ Da) can enhance angiogenesis by stimulating endothelial cell proliferation, increase their matrix collagen production or direct the synergistic effect of VEGF on angiogenesis (Montesano *et al.*, 1996; Rooney *et al.*, 1993; Slevin *et al.*, 2002). Combining fibrin and HA can provide mutual advantages both physiologically and biologically.

Recently, chemically modified HA and fibrinogen have been reported to strengthen the stability of hydrogel (Lee and Kurisawa, 2013; Loebel *et al.*, 2019; Snyder *et al.*, 2014). However, modifying HA and fibrinogen needs chemical reactions, complicating the preparation processes and brings additional unpredictable effects in clinical applications such as implants. By contrast, naturally derived HA and autologous fibrinogen has been widely used in clinical orthopaedic applications (Bannuru *et al.*, 2009; Huskisson and Donnelly, 1999; Tayapongsak *et al.*, 1994). Also, fibrin-HA hydrogels have been applied to cell regeneration or differentiation studies, aiming at solving different clinical problems (Arulmoli *et al.*, 2016; Häckel *et al.*, 2019). In the current study, a hydrogel scaffold was developed for *in vitro* vascularisation with great biocompatibility. The gels can also be utilised for *in vivo* applications. The developed hydrogel was mainly composed of fibrinogen. Naturally derived high-molecular-weight HA (HMWHA, Molecular Weight ~$1.5\text{-}1.8 \times 10^6$ Da) was added to improve the mechanical properties for vascularisation promotion and mechanical stability, this also has the potential for clinical application use. Angiogenic growth factors, vascular endothelial growth factor (VEGF) and basic fibroblast growth factor (bFGF) were also added to the hydrogel. The additional growth factors could cooperate with the fibrin and ECM molecules to help endothelial cells differentiate and sprout (Battegay, 1995; Bischoff, 1995; Sahni and Francis, 2000; Sahni *et al.*, 1998; Schenk *et al.*, 1999). In the experiments, the vascularisation performance of the hydrogels was characterised using image analysis of both *in vitro* cell culture and *in vivo* mouse models. The mechanical properties of the hydrogels were also characterised using atomic force microscopy (AFM).

The obtained results confirmed that the developed HA-supplemented fibrin hydrogel, a biocompatible and degradable 3D scaffold, could provide a suitable environment for endothelial cell differentiation both *in vitro* and *in vivo*, as well as the mechanical strength needed for practical applications. Fibrinogen, which can be extracted from patient's own blood, is a suitable material for autologous transplantation and is successfully used for many clinical surgeries (Gestring and Lerner, 1983; Haisch *et al.*, 2000). In addition, HA is widely applied in clinical situations, especially for osteoarthritis treatments (Bannuru *et al.*, 2009; Huskisson and Donnelly, 1999). The developed hydrogel has great potential to be directly applied

in clinical research and may provide a promising solution for inadequate vascularisation of bulk transplants.

Materials and Methods

Cell culture

In order to study vasculogenesis both *in vitro* and *in vivo*, as shown in Fig. 1, commercially available human umbilical vein endothelial cells (HUVECs) (CC-2519, Lonza Group, Basel, Switzerland) were used for this study. The cells were cultured and expanded in endothelial growth medium (EGM-2) (CC-3162, Lonza Group). For consistent results, only cells with passage numbers 4 to 6 were used. The stock of cells was maintained in a humidified cell incubator (HERAcell 240i, Thermo Fisher Scientific Inc., Waltham, MA, USA) at 37 °C and 5 % CO_2.

Hydrogel preparation

For the 3D matrix supporting the endothelial cell growth and networking, hydrogels both with and without endothelial cells were prepared. Two types of hydrogels were prepared: fibrinogen hydrogel (F-Gel) and fibrinogen-HA hydrogel (FH-Gel). In order to mix the endothelial cells within the hydrogels, the HUVECs were detached using TrypLE express enzyme (12604, Life Technologies, Grand Island NY, USA) and then washed with the complete medium to inactivate the TrypLE. The cells were then resuspended in the medium before mixing with the hydrogel. The hydrogel solutions were prepared prior to cross-linking with thrombin. The hydrogel solution for F-gel contained a final concentration of: 8 mg/mL fibrinogen (F8630, Sigma, St. Louis, MO, USA), 40 ng/mL VEGF (100-20, Pepro Tech, Rocky Hill, NJ, USA), 40 ng/mL β-FGF (100-18B, Pepro Tech). The hydrogel solution for FH-gel contained a final concentration of 8 mg/mL fibrinogen, 40 ng/mL VEGF, 40 ng/mL β-FGF and 0.05 % (w/v) hyaluronic acid (53747, Sigma). For the hydrogel with the cells, HUVECs with final density of 4×10^5 cells/mL were mixed into the hydrogel. Each well of the 48-well culture plate were filled with the 300 µL hydrogel solution and then 24 µL 0.5 mg/mL thrombin (T4648, Sigma, St. Louis, MO, USA) was added for hydrogel formation. The plate was kept at 37 °C for 30 min for gel formation before filling each well with medium. The plate was then allowed incubation at 37 °C, 5 % CO_2 for 7 d.

Hydrogel material property characterisation

In order to examine mechanical strength of the hydrogel and determine the Young's modulus of the fibrin gels, biological AFM (bio-AFM) was applied (Fig. 2**a**). Atomic force microscopy (AFM) is a form of scanning probe microscopy that uses precisely

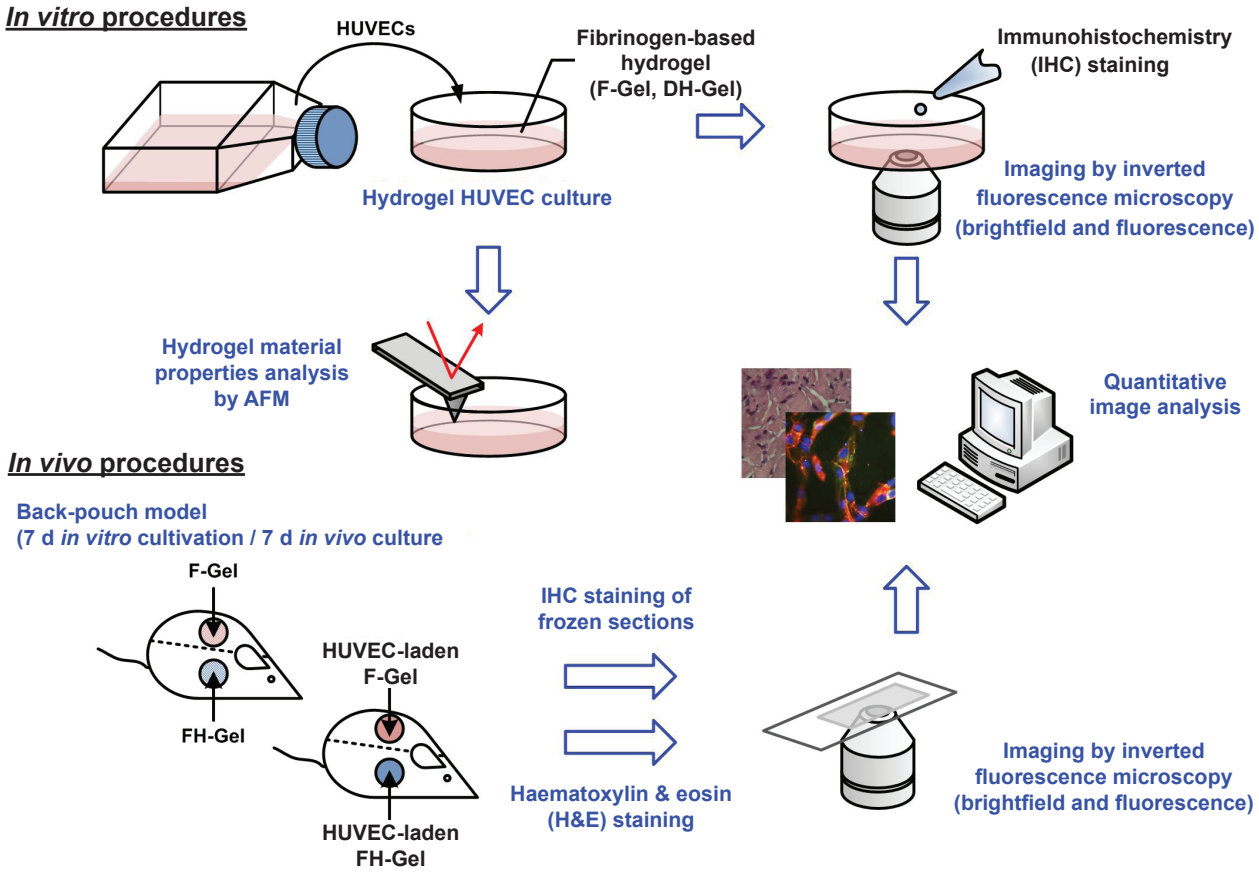

Fig. 1. Schematics of the process for the *in vitro* and *in vivo* experiments to study vessel formation by endothelial cells cultured in hydrogels with different compositions.

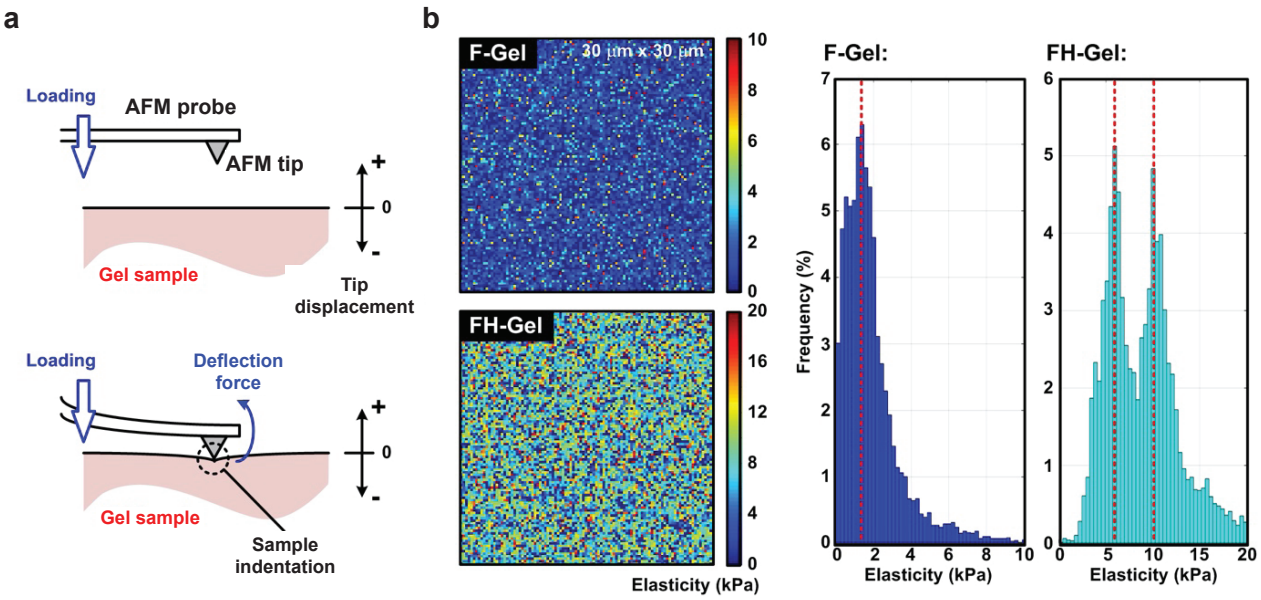

Fig. 2. Elasticity test of hydrogels. (**a**) The AFM measurement setup exploited to characterise the mechanical properties of the hydrogels. (**b**) AFM measurement results. The spatial distribution of the elasticity values obtained from AFM measurements on 30 μm × 30 μm (100 × 100 data points) hydrogel samples, and the histograms of the elasticity values.

manufactured probes that can scan sample surfaces at sub-nm resolution. One of the notable features of an AFM probe is the spring-like cantilever with a sharp tip attached for contact investigation of a specimen's mechanical properties (Lu *et al.*, 2006; Rico *et al.*, 2005). Among contact-mechanics theories, the Hertz model (Hertz) gives the normal contact load as a function of local deformations of the indented specimen. The measured elastic properties of the specimen, such as Young's modulus and relevant geometrical effects, have been widely employed in indentation hardness tests. Accordingly, elastic properties of specimen surfaces, to which the probe cantilevers are highly sensitive, can be quantitatively evaluated by collecting force-displacement indentation curves during raster scanning. A number of studies have also attempted to characterise elastic properties of biomaterials through AFM indentation approaches at specific spots on the scanned surface (Cross *et al.*, 2007; Docheva *et al.*, 2008; Engler *et al.*, 2006; Lin *et al.*, 2016; Rico *et al.*, 2005). In the current study, the sample elasticities were measured through the force spectroscopy settings of the feedback set point (100 nN, extension speed: 1 μm/s; relative spectroscopy set point of 450 nN), implemented on a conventional bio-AFM system (NanoWizard 3, JPK Instrument AG, Berlin, Germany) using a four-sided pyramid tip attached to the probe with a spring constant of 7.4 N/m and half edge-angle of 11.25° (PPP-NCSTR, Nanosensors) for each indentation spot at ambient temperature. Afterwards, the collected indentation curves were processed using AFM data processing software (JPK DP 4.2, JPK Instrument AG, Berlin, Germany) to extract the desired best-fitting Young's modulus of the Hertz model on the raw data, with a material Poisson's ratio value of 0.5. Consequently, using an AFM probe to indent the fibrin gel substrate, the testing force curves were obtained and then used for the least-squares fitting calculation, based on the contact-mechanics theory, to yield the desired elastic modulus of the substrate material.

Hydrogel *in vivo* transplantation

For the *in vivo* experiments, male nude mice (BALB/c NU) with ages of 5-6 weeks were purchased (BioLASCO, Taipei, Taiwan). The animal studies were conducted under the permission issued by animal ethics committee of Taipei Veterans General Hospital and all procedures were performed under supervision of the committee. After being housed in cages for 1-2 weeks, the animals were anaesthetised by intraperitoneal injection of 5 % 2,2,2-Tribromoethanol (T48402, Sigma-Aldrich, St. Louis, MO, USA). Two subcutaneous pockets were produced by dissection on each dorsal side of the mouse, where the 3D hydrogels were placed. The incisions were closed with a surgical suture. Hydrogels without the HUVECs were also implanted as controls. The hydrogels were cultured in the mice for 7 d, and then the mice were sacrificed by CO_2 inhalation. The hydrogel samples were removed from the mice and then fixed with formalin for haematoxylin and eosin (H&E) staining or immersed in Dulbecco's phosphate-buffered saline (DPBS, 14190, Invitrogen Corp, UK) for immunofluorescence staining. Twenty-four mice were used, 6 for each group.

H&E staining

In order to visualise the blood vessel formation within the hydrogels, H&E staining was performed on the *in vivo* samples. The hydrogel samples from the *in vivo* transplantations were first fixed with formalin before processing into paraffin wax (Leica Biosystems). Serial 5 μm sections were cut and 3 sections were mounted on glass slides (Muto Pure Chemicals Co., Ltd.; Tokyo). The mounted sections were oven dried for 30 min at 60 °C, and then the slides were stained with H&E (Leica Auto Stainer XL, Leica Microsystems, Buffalo Grove, IL). Cover slips were automatically mounted on the stained sections using xylene containing rapid mounting medium Entellan (107961, Merck, Darmstadt, Germany) and stored at room temperature.

Immunofluorescence staining

In order to further confirm the vascularisation of the endothelial cells and investigate the *in vivo* cell origin, immunofluorescence staining was performed. For the *in vitro* material within the hydrogels, stainings targeting VE-cadherin, F-actin and nucleus were carried out after 7 d in culture. After washing with DPBS, gel samples were fixed in 4 % paraformaldehyde (158127, Sigma-Aldrich) in DPBS for 15 min, then permeabilised using 0.1 % Triton X-100(T9284, Sigma-Aldrich) in DPBS for 5 min. After blocking using Image-iT FX signal enhancer (I36933, Invitrogen, Carlsbad, CA, USA) for 30 min, gel samples were incubated overnight at 4 °C with goat anti-human VE-cadherin (SC6458, Santa Cruz Biotechnology, Santa Cruz, CA, USA). The samples were then incubated for 1 h with Alexa Fluor 488 Donkey anti-goat IgG (A11055, Invitrogen,) as a secondary antibody. For staining F-actin and nuclei, the cells were stained with Alexa Fluor 594 Phalloidin (A12381, Invitrogen) for 1 h and DAPI (D9542, Sigma-Aldrich) for 10 min.

For the *in vivo* samples, staining targeting both von Willebrand (VW) factor and nuclei was carried out. Hydrogel samples from the *in vivo* transplantation were immersed in DPBS and frozen sectioning performed immediately. Four × 2 μm serial frozen sections were cut using a cryostat (Microm HM 550, Thermo, Walldorf, Germany) with a clean blade, and 3 sections of each set were mounted on glass slides (Muto Pure Chemicals, Tokyo, Japan). The unfixed sections were immediately stored at −20 °C. The frozen sections were thawed at room temperature for 30 s, without drying, and immersed immediately in 4 % paraformaldehyde in DPBS for 10 min. After fixation, 0.1 % Triton X-100 in DPBS was applied for 3 min for permeabilisation. Using 1 % BSA (A7906, Sigma-Aldrich) as blocking buffer for 1 h, the samples were then incubated with Anti-VW Factor (ab6994, Abcam, Cambridge, UK) for 2 h at room temperature. Thereafter, the samples were incubated for 1 h with Alexa Fluor 568 goat anti-rabbit IgG (H+L) (A11011, Invitrogen), as a secondary antibody. For revealing nuclei, DAPI staining was applied for 10 min.

Image analysis

For quantitative comparison of the results obtained during treatment under different conditions, both two- and three-dimensional microscopy imaging and analysis were performed. The hydrogel samples containing the cells were imaged using an inverted fluorescence microscope (AF7000, Leica Microsystems, Solms, Germany) and a confocal microscope (TCS SP5, Leica Microsystems) following immunofluorescence staining. To obtain images of planes at various depths within the samples, Z-stack images were set to be captured every 100 μm. The images were then analysed using MetaMorph NX software for offline analysis and angiogenesis application module packages (MetaMorph® NX 2.0, Universal Imaging Corporation, West Chester, PA, USA).

Results

AFM measurement

The mechanical properties of the hydrogels were first characterised using AFM. In order to eliminate the bias from local measurements, samples over an area of 30 × 30 μm^2 were indented with 100 × 100 data points to ensure the measured results were representative. Fig. 2(**b**) shows the elasticity distribution within the measured area and the histograms of the estimated elasticity values. The measurement results showed that the F-Gel had relatively consistent elasticity values over the measured area with the value of 1.3 kPa at the highest frequency, and an average elasticity was 1.86 kPa. In contrast, the distribution of elasticity values of the FH-Gel had 2 major groups with values of 5.8 and 10.0 kPa at higher frequencies. The average elasticity value was 8.79 kPa. The results suggested that the AFM measurement could provide meaningful and representative results for hydrogel elasticity estimation. FH-Gel had about 3.7 × higher average elasticity than F-Gel that may have resulted from being supplemented with HA.

***In vitro* immunofluorescence staining**

Immunofluorescence staining was first performed to investigate the cellular morphology and behaviour within the hydrogels *in vitro*. Fig. 3(**a**,**b**) show both brightfield and fluorescence images of the endothelial cells cultured in both F-Gel and FH-Gel at different time points (days 0, 3, 7, 10 and 15). To study the cellular network, the cells were stained for the endothelial-cell-specific tight-junction protein, vascular endothelial cadherin (VE-cadherin) and cytoskeleton protein F-actin after 3, 7 and 10 d in culture. The green and red fluorescence indicated positive identification of VE-cadherin and F-actin in the HUVECs cultured in both hydrogels. Cell nuclei stained with DAPI, showing blue fluorescence, indicated the distribution of the HUVECs within the hydrogels. The VE-Cadherin was localised at the cell periphery while the F-actin was initially distributed

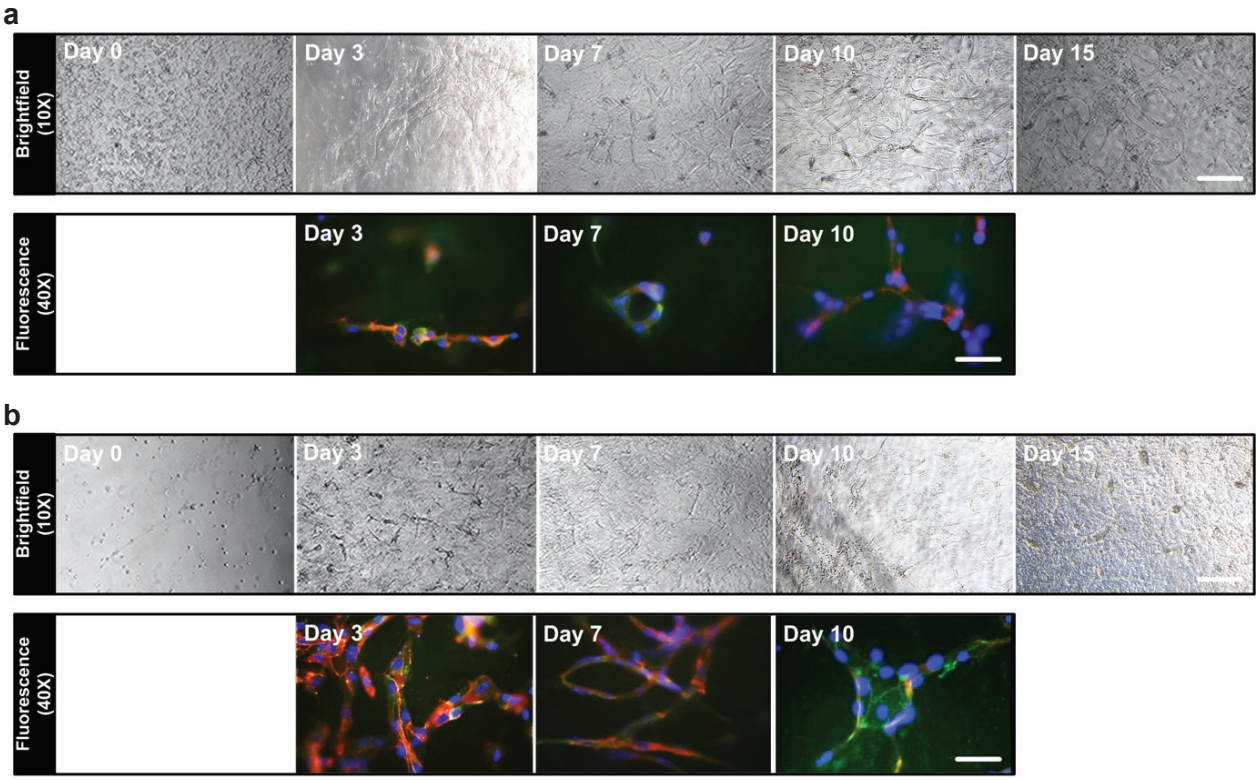

Fig. 3. Vasculature morphogenesis within the gels. (**a**) and (**b**) Brightfield and fluorescence images of the endothelial cells cultured in the F-Gel and FH-Gel at different days, respectively. The cells are immunofluorescence stained for F-actin (red), VE-Cadherin (green) and nuclei (blue). Scale bars in the brightfield and fluorescence images are 200 and 50 μm, respectively.

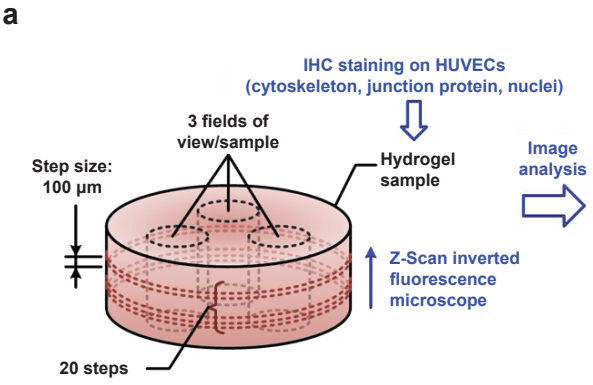

b

Parameter	Definition
Total tube length	Total μm of vessel length (excluding nodes)
Mean tube length	Total length divided by the number of segments
Average tube thickness	Average thickness of vessels computed as total area (excluding nodes) divided by total length in μm

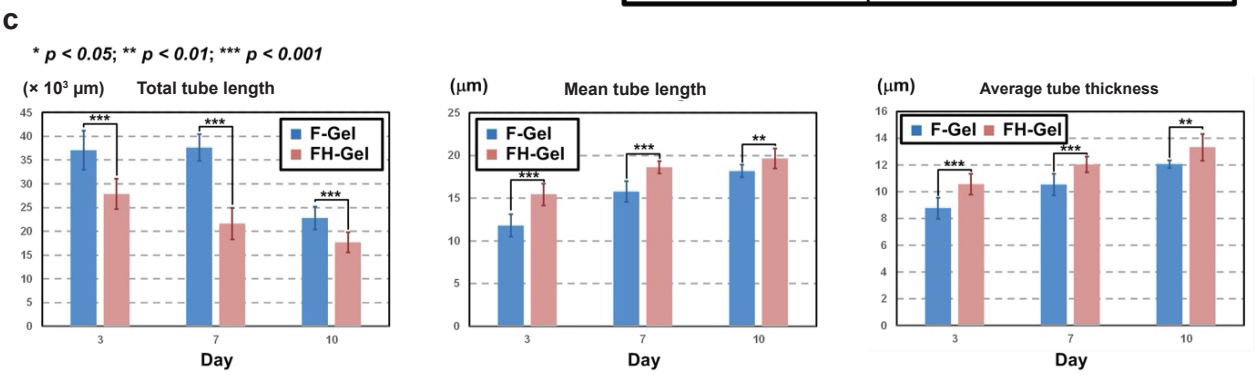

Fig. 4. Quantitative tubulogenesis assay. (**a**) Three-dimensional imaging. The setup and parameters exploited for the 3D imaging of the collected samples from the *in vitro* experiments. (**b**) Analysis parameters. The parameters analysed using the Metamorph NX 2.0 software with the angiogenesis tube formation module. (**c**) *In vitro* cell culture quantitative analysis. Unpaired student *t*-tests were performed to statistically analyse the results obtained from F-Gel and FH-Gel at different days ($n = 3$).

uniformly across the cells and later, following culturing, localised at the periphery. The images confirmed that the HUVECs were differentiated into vascular endothelial cells and formed 3D vessel networks.

The collected 3D fluorescence images from the *in vitro* studies, and analysed using the automated microscopy and image software (Metamorph NX 2.0), with an angiogenesis tube formation module with specific parameters (Fig. 4**a**,**b**), showed quantitative analysis (Fig. 4**c**). First, the total tube lengths – defined as total vessel length in μm, excluding nodes – formed by the HUVECs when cultured in different hydrogel compositions were calculated. The tubes were automatically identified by the software, and the results from the images analysed at days 3, 7 and 10 were plotted. The total tube lengths in the F-Gel were 33.2 %, 74.1 % and 28.9 % longer than those in the FH-Gel at days 3, 7 and 10, respectively. The total length decreased during culture in both F-Gel and FH-Gel. The total length decreased from day 3 to 10 by approximately 38.5 % in the F-Gel, and about 36.5 % in the FH-Gel.

In order to quantitate the 3D networking formation of the HUVECs, the mean tube length – defined as total length divided by the number of segments – was also analysed. Mean tube lengths at days 3, 7 and 10 for the HUVECs cultured in FH-Gel were 30.8 %, 17.9 % and 8.1 % longer than those in F-Gel, respectively. The observation was the opposite of that obtained for the total tube-length analysis. Furthermore, the mean tube lengths increased in both F-Gel and FH-Gel during culture, which was also opposite to the trend for the total tube-length analyses. The mean tube lengths at days 3 to 10 increased approximately 54.1 % and 27.3 % for the HUVECs cultures in F-Gel and FH-Gel, respectively.

To further investigate the morphology of the formed networks, average tube thickness – computed as total area divided by total length – was calculated to seek the possible reasons for the opposite trends obtained in the total and mean tube length analyses. The average tube thicknesses for the HUVECs cultured in the FH-Gel were 20.6 %, 14.3 % and 10.5 % higher than those in the F-Gel at days 3, 7 and 10, respectively. Also, the average thicknesses increased in both F-Gel and FH-Gel during culture. These were similar trends to those obtained for the mean tube-length analyses. The average tube thicknesses increased approximately 37.6 % and 26.2 % from day 3 to 10 for the HUVECs cultures in the F-Gel and FH-Gel, respectively.

In vivo H&E staining

In order to demonstrate the performance of the hydrogel culture for practical clinical applications, *in vivo* studies using the mouse back-pouch models (Fig. 5**a**) were also conducted. After the transplantation and 7 d culture in the mice, the samples were extracted from the animals and fixed immediately. The samples were stained with H&E after embedding in paraffin-wax blocks and cutting into serial sections. Fig. 5(**b**) shows the images of the H&E stained cells in the hydrogels. The cell nuclei showed a blue-purple colour, the hydrogel matrices were pink, and the vessel networks created by the cells displayed as white areas. The H&E stained cell images show the distribution and structures of the cells in the F-Gel and FH-Gels. The results provided the layouts of the vessel networks in single slices of the hydrogels and showed the network structure of the cells *in vivo*.

Quantitative analysis was carried out on images of single slices of the H&E stained samples (Fig. 5**c**). The green-colouring shows the tube areas, as automatically identified by the software. The plots show the calculated total area and cell number per unit area for different experiments. Since the images obtained from the H&E stained samples provided tube formation information on a single slice, the total tube area within a unit area (1 mm^2) was first analysed. The total tube area within the hydrogels with HUVECs were much higher (7.2 × in F-Gel, and 8.8 × in FH-Gel) than those within the hydrogels without HUVECs. The difference between the areas within the F-Gel and FH-Gel without HUVECs was not significant. In contrast, for the hydrogels with HUVECs, the area within the FH-Gel was 51.6 % higher than that within the F-Gel.

To quantify the cells in the hydrogels, cell numbers in the H&E stained images of single slices were also analysed by the software. Cell numbers in the FH-Gel and F-Gel with HUVECs were 3.2 and 2.8 × higher than those in the gels without the cells, respectively. After the *in vivo* culture, the cell nuclei could be observed in the hydrogels without HUVECs, and the cell number in the FH-Gel was approximately 25.7 % higher than that in F-Gel. The results suggested that the mouse cells could be recruited into the hydrogels after their insertion, and the HA supplementation enhanced the number of mouse cells recruited. Similar to the total area analysis, the cell number in the FH-Gel was 38.8 % higher than that in the F-Gel, indicating the better proliferation of HUVECs within the FH-Gel.

In vivo immunofluorescence staining

Since the H&E stained images could only provide information on tube formation in single slices, immunofluorescence staining with widefield microscopy was exploited for imaging the *in vivo* samples. To further distinguish between the HUVECs and mouse cells, immunofluorescence staining was also performed. The extracted samples were stained for a blood glycoprotein von Willebrand factor (VWF) and nuclei (DAPI). The VWF was chosen to be specifically bound to the human cells for identification of HUVECs introduced into the hydrogels before the implantation. Fig. 6(**a**) shows the fluorescence images of the hydrogels collected after 7 d implantation in the mice. The images show that the human-cell-specific fluorescence VWF staining can be observed in both with and without HUVECs

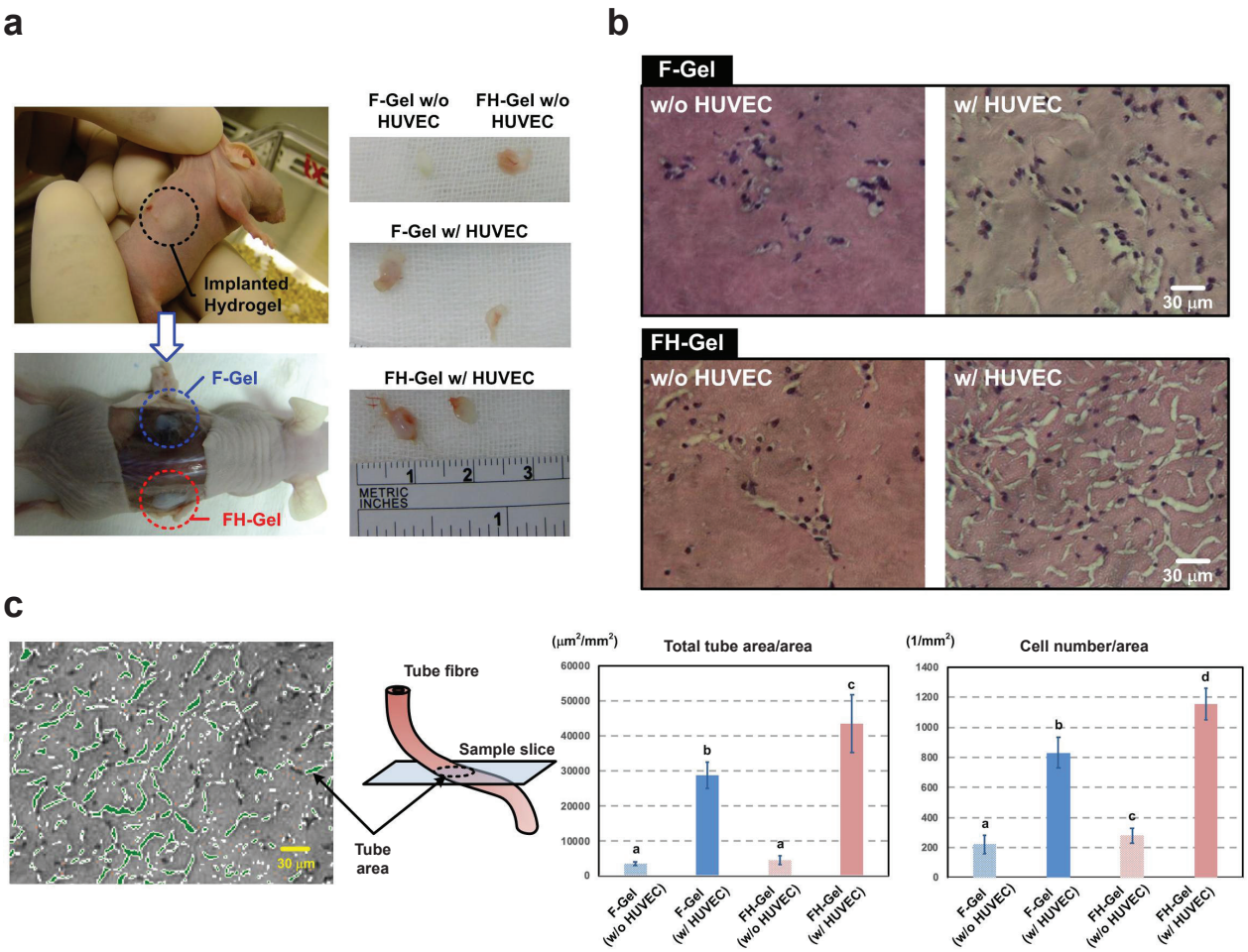

Fig. 5. Histology and quantitative assay of *in vivo* study. (**a**) Images of the back-pouch model used in the *in vivo* experiments and the collected samples. (**b**) H&E stained images of the hydrogels collected from the *in vivo* experiments. (**c**) The quantitative analysis procedure and the obtained quantitative results from the hydrogels with different compositions. The significantly different results statistically analysed using the analysis of variance (ANOVA) are designated with different letters (a, b, c, d = $p < 0.05$).

samples, suggesting optical imaging artifacts and non-specific bonding of the proteins onto the non-human organelles. Despite of the undesired signals, the HUVECs could still be clearly imaged using the VWF staining in the hydrogel samples with HUVECs. In addition, the cell nuclei of the cells, with and without expressing VWF, could be observed indicating that both human and non-human cells could be clearly identified in the images. As a result, the HUVECs and mouse cells could be successfully distinguished based on the images stained with the VWF and DAPI fluorescence.

Fig. 6(**b**) shows the quantitative analysis results from the collected *in vivo* fluorescence images. Tube lengths, defined as total length of the object assuming that it is a tube within a specific area (1 mm^2), were first calculated. The objects were automatically identified by the software. The results of the image analyses of the hydrogels both with cells and without cells were collected. The plot shows that the total tube lengths of the FH-Gel and F-Gel with the cells were approximately 1.2 and 1.8 × longer than those of the gels without the cells, respectively. Comparing with the hydrogels without cells, the tube length in the FH-Gel was 98.2 % longer than that in the F-Gel. In addition, the tube length in the FH-Gel with cells was 55.9 % longer than that in the F-Gel with cells. The length difference between the without and with HUVECs in FH-Gel is 32.2 % higher than that in F-Gel. In summary, the total tube lengths in the FH-Gel were longer than those in the F-Gel. It was noted that the result was opposite to that obtained in the *in vitro* total-tube-length analysis; however, similar to the total area variation obtained in the H&E stain study.

The average tube length, defined as total length of the object – assuming that it is a tube – divided by object number, was also analysed for the *in vivo* experiments based on the collected fluorescence images. After the *in vivo* culture, average tube lengths in the FH-Gel and F-Gel with cells were 95.7 % and 34.4 % longer than in the gels without cells, respectively. However, there was no significant difference between the average lengths obtained from

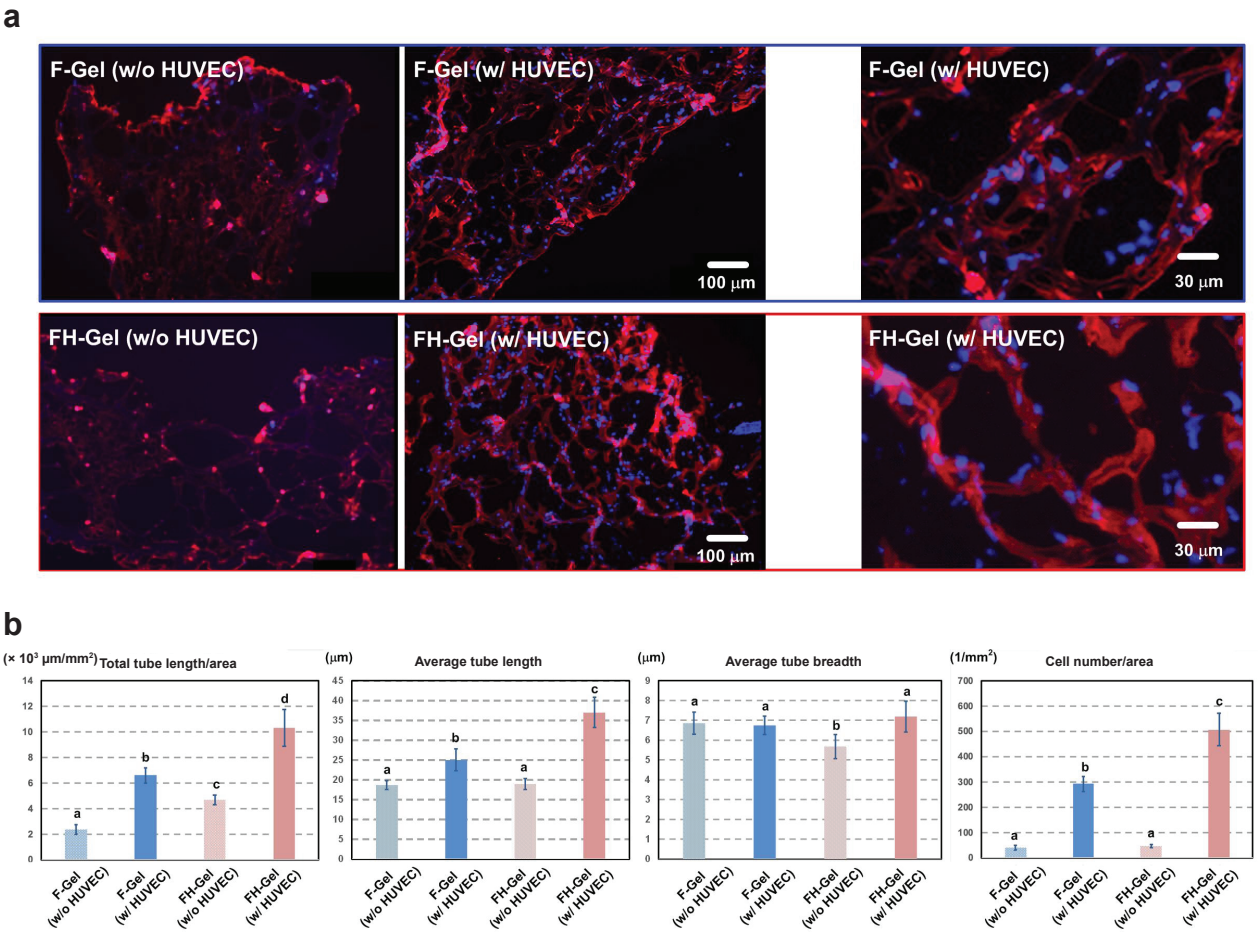

Fig. 6. Fluorescence images and quantitative assay of *in vivo* study. (**a**) The fluorescence images obtained from the *in vivo* experiments, in which the cells were stained with VWF (red) for human and nuclei (blue) for human and mice. (**b**) The quantitative analysis results obtained in the *in vivo* experiments from the hydrogels with different compositions. The significantly different results statistically analysed using the analysis of variance (ANOVA) are designated with different letters (a, b, c, d = $p < 0.05$).

the FH-Gel and F-Gel without cells. The average tube length of FH-Gel with cells was 47.7 % higher than F-Gel with cells. In addition, after subtracting the lengths from those in the hydrogels without cells, the average length in the FH-Gel was 1.8 × longer than that in the F-Gel. The trend was similar to that obtained from the mean-tube-length and total-tube-length analyses in the *in vitro* and *in vivo* experiments, respectively.

Similar to the tube-thickness analysis for the *in vitro* experiments, average tube breadth – calculated as width of the object assuming that it is a tube then divided by object number – was also analysed on the fluorescence images obtained from the *in vivo* experiments. Average tube breadth in the FH-Gel without cells was 17.2 % lower than F-Gel without cells. FH-Gel with cells was 26.4 % higher than FH-Gel without cells, but there was no significant difference between F-Gel and its control gel. The average tube breadth in the FH-Gel was 6.6 % higher than F-Gel. FH-Gel was also shown to be 13.6 × higher than F-Gel after subtracting the control gel values. The results had similar trends to the *in vitro* average tube thickness analyses.

To study the interaction between the hydrogels implanted into the mice and the host, cell numbers were analysed by the software. After the *in vivo* culture, nuclei number was counted by the software in the same way as the cell numbers were determined in the hydrogel samples. Cell numbers in the FH-Gel and F-Gel with cells were 9.9 and 6.5 × higher than those in the hydrogels without the cells, respectively. After implanting into the mice and 7-day cultures, the nuclei could be found in both the FH-Gel and F-Gel without cells samples. The cell numbers in the FH-Gel were 18.4 % higher than that in the F-Gel without cells. Moreover, the cell numbers in the FH-Gel were 73.1 % higher than that in the F-Gel. In addition, after subtracting the cell numbers in the hydrogels without the cells, the cell number in the FH-Gel with cells was 81.6 % higher than that in the F-Gel with cells. The results showed that the cell numbers were higher in the FH-Gel than in the F-Gel after the *in vivo* implantation.

Discussion

The *in vitro* tube-formation quantitative analysis revealed an increase of the mean tube length and average tube thickness during cultivation in both gels. On the other hand, the total tube length after the culture was decreased. The results suggested that the development of vasculature networks mainly relied on HUVEC morphogenesis in the 3D ECM hydrogel instead of proliferation. Studies have shown that fibrin-based hydrogels allow for continually releasing impregnated growth factors, thus supporting cell spreading and migration (Brown *et al.*, 1996; Sahni and Francis, 2000; Sahni *et al.*, 1998; Wong *et al.*, 2003). During the process, the cells collectively migrate toward each other to form VE-cadherin positive endothelium and further assemble into vessels. The HMWHA has been reported as an anti-angiogenic factor inhibiting vascularisation; however, it can also increase the porosity of fibrin hydrogel and stimulate the cell migration within the 3D structure (Genasetti *et al.*, 2008; Hayen *et al.*, 1999; Komorowicz *et al.*, 2017; Maharjan *et al.*, 2011; Rooney *et al.*, 1995). In addition, HMWHA can trigger endothelial cell growth and motility activation (Bourguignon *et al.*, 2001; Vigetti *et al.*, 2008; Weigel *et al.*, 1988). In the current study, the differences between the F-Gel and FH-Gel experiments indicated that the addition of HMWHA did affect the HUVECs vascularisation within the 3D matrix. The results showed that the presence of HMWHA increased mean tube length and tube thickness instead of total tube length. In other words, it suggested that the net effect of adding HMWHA could be the improving of vascularisation by enhancing the architecture and robustness of the vasculature rather than its total amount.

In the *in vivo* experiments, the addition of HMWHA did promote cell proliferation and vasculogenesis, as evidenced by the histology with increased total tube area and cell number, which was not seen in the *in vitro* study. This discrepancy could result from the lack of a wound-repair mechanism, caused by the implantation procedure and supportive system from host tissue, in the *in vitro* study. The implanting procedures can induce influx of resident cells that produce cytokines and promote endothelial cell migration and proliferation (Rollwagen *et al.*, 1993; Spargo *et al.*, 1994). The recruitment of the mice cells into the hydrogels could further supply the cytokines to promote the HUVEC proliferation within the pre-seeded HUVECs. In the *in vivo* study, the hydrogels without pre-seeding of HUVEC, the cell numbers in the retrieved FH-Gel was higher than that in the F-Gel. The higher cell numbers in FH-Gel with HUVECs may have resulted from the promoted mouse cell recruitment and the HUVEC proliferation due to the addition of HMWHA. HMWHA plays an important role in inducing cell migration to the wounded site and also interacts with fibrin to facilitate the wound-healing process (Weigel *et al.*, 1988; Weigel *et al.*, 1986). HMWHA can also stabilise the fibrin hydrogel to prevent fibrinolysis and provide better mechanical support (Komorowicz *et al.*, 2017; LeBoeuf *et al.*, 1987; LeBoeuf *et al.*, 1986). Therefore, FH-Gel facilitated a wound repair reaction to influx more resident cells and HUVEC proliferation than F-Gel.

In addition, the promoted cell proliferation and vasculogenesis may result from additional space created in the FH-Gel due to HMWHA dissociation. It has been reported that HMWHA has higher binding affinity to fibrin than low molecular HA and can form an IPN structure with fibrin (LeBoeuf *et al.*, 1986; Yu *et al.*, 2015). HA networks can be embedded and distributed within the fibrin with large interconnected pores. As a result, HA can stably maintain within the hydrogel and keep its integrity *in vitro* for more than 2 weeks (Park *et al.*, 2005; Yu *et al.*, 2015). In the *in vivo* situation, since the HA is not covalently bound to fibrin within the hydrogel, HA may be dissociated from the hydrogels generating additional porosity. Therefore, the HA dissociation may play a role making more additional spaces in the FH-Gel than in the F-Gel, as observed following H&E staining. This may also explain the discrepancy between the results obtained from the *in vitro* and *in vivo* experiments. Furthermore, image analysis artefacts may also be a limiting factor for accurate analysis. The vessel regions were automatically selected by the software, and then manually checked after the selection. However, the presumed vessel space, as selected by the software, was not simultaneously labelled as validated with specific vessel markers. Therefore, the areas attributed to the HA dissociation and the analysis artefacts may also be included in the results.

By examination of the fluorescence images obtained in the *in vivo* study, the promotion of cell proliferation and blood vessel network formation can also be confirmed from the observed increase of total and average tube lengths. However, the addition of HMWHA does not greatly affect the tube breadth following the tube formation. With help of the HMWHA, the wound healing process accelerates and recruits more cells into the gel to provide cytokines (Rollwagen *et al.*, 1993; Spargo *et al.*, 1994; Weigel *et al.*, 1986). Furthermore, the pre-seeded HUVECs within the hydrogels can help to deliver positive effects on further vasculogenesis. The proliferation and vessel networking of all sources of endothelial cells can be further accelerated after implantation. For practical sample handling, the higher elasticity of the FH-Gel compared to the F-Gel provided better mechanical stability. Hydrogels with greater elasticity possess more deformation-resistant ability in response to flowing blood (Weisel, 2007). The AFM measurement confirmed that it has about 3.7 × higher average elasticity than F-Gel resulting from the addition of HA. As a result, the higher mechanical strength of FH-Gel makes it more reliable for practical clinical usage.

Conclusion

Vasculogenesis within natural fibrin-based hydrogels, with and without HA supplementation, was studied using *in vitro* cell culture and *in vivo* animal models. In the *in vitro* study, the HUVECs were exploited as a model cell line to investigate vasculogenesis within the hydrogels. From the experimental results, the developed hydrogels with added HA were observed to promote vasculogenesis in both *in vitro* and *in vivo* models. In addition, the recruitment of the cells from the host animals also increased when the hydrogels with HA were implanted, and the HUVEC embedding could promote the vasculogenesis *in vivo*. The material characterisation showed that hydrogel elasticity was increased by adding HA, giving the great mechanical strength that is desired for practical clinical applications. The developed fibrin-based natural hydrogel provided a foundation for easy preparation, great biocompatibility and better vascularisation to overcome the current challenges and also possesses great potential for *in vivo* implantation applications.

Acknowledgments

This paper is based on work supported by the Taiwan National Science Council (NSC 102-2314-B-075-014), Taipei Veterans General Hospital (V102-113), Taiwan Ministry of Science and Technology (MOST 107-2628-E-001-003-MY3), and Academia Sinica Career Development Award (AS-CDA-106-M07).

References

Arulmoli J, Wright HJ, Phan DT, Sheth U, Que RA, Botten GA, Keating M, Botvinick EL, Pathak MM, Zarembinski TI (2016) Combination scaffolds of salmon fibrin, hyaluronic acid, and laminin for human neural stem cell and vascular tissue engineering. Acta biomater **43**: 122-138.

Bannuru RR, Natov NS, Obadan IE, Price LL, Schmid CH, McAlindon TE (2009) Therapeutic trajectory of hyaluronic acid *versus* corticosteroids in the treatment of knee osteoarthritis: A systematic review and meta-analysis. Arthritis Rheum **61**: 1704-1711.

Battegay E (1995) Angiogenesis: mechanistic insights, neovascular diseases, and therapeutic prospects. J Mol Med (Berl) **73**: 333-346.

Bischoff J (1995) Approaches to studying cell adhesion molecules in angiogenesis. Trends Cell Biol **5**: 69-74.

Bourguignon LY, Zhu H, Shao L, Chen Y-W (2001) CD44 interaction with c-Src kinase promotes cortactin-mediated cytoskeleton function and hyaluronic acid-dependent ovarian tumor cell migration. J Biol Chem **276**: 7327-7336.

Brown KJ, Maynes SF, Bezos A, Maguire DJ, Ford MD, Parish CR (1996) A novel *in vitro* assay for human angiogenesis. Lab Invest **75**: 539-555.

Brown KL, Cruess RL (1982) Bone and cartilage transplantation in orthopaedic surgery. A review. J Bone Joint Surg Am **64**: 270-279.

Cross SE, Jin Y-S, Rao J, Gimzewski JK (2007) Nanomechanical analysis of cells from cancer patients. Nat Nanotechnol **2**: 780-783.

Curl WW, Krome J, Gordon ES, Rushing J, Smith BP, Poehling GG (1997) Cartilage injuries: a review of 31,516 knee arthroscopies. Arthroscopy **13**: 456-460.

Docheva D, Padula D, Popov C, Mutschler W, Clausen-Schaumann H, Schieker M (2008) Researching into the cellular shape, volume and elasticity of mesenchymal stem cells, osteoblasts and osteosarcoma cells by atomic force microscopy. J Cell Mol Med **12**: 537-552.

Engler AJ, Sen S, Sweeney HL, Discher DE (2006) Matrix elasticity directs stem cell lineage specification. Cell **126**: 677-689.

Genasetti A, Vigetti D, Viola M, Karousou E, Moretto P, Rizzi M, Bartolini B, Clerici M, Pallotti F, De Luca G (2008) Hyaluronan and human endothelial cell behavior. Connect Tissue Res **49**: 120-123.

Gestring GF, Lerner R (1983) Autologous fibrinogen for tissue-adhesion, hemostasis and embolization. Vasc Endovascular Surg **17**: 294-304.

Gibot L, Galbraith T, Huot J, Auger FA (2010) A preexisting microvascular network benefits *in vivo* revascularization of a microvascularized tissue-engineered skin substitute. Tissue Eng Part A **16**: 3199-3206.

Grassl E, Oegema T, Tranquillo R (2002) Fibrin as an alternative biopolymer to type-I collagen for the fabrication of a media equivalent. J Biomed Mater Res **60**: 607-612.

Haisch A, Loch A, David J, Pruss A, Hansen R, Sittinger M (2000) Preparation of a pure autologous biodegradable fibrin matrix for tissue engineering. Med Biol Eng Comput **38**: 686-689.

Hayen W, Goebeler M, Kumar S, Rießen R, Nehls V (1999) Hyaluronan stimulates tumor cell migration by modulating the fibrin fiber architecture. J Cell Sci **112**: 2241-2251.

Häckel S, Zolfaghar M, Du J, Hoppe S, Benneker LM, Garstka N, Peroglio M, Alini M, Grad S, Yayon A (2019) Fibrin-hyaluronic acid hydrogel (RegenoGel) with fibroblast growth factor-18 for *in vitro* 3D culture of human and bovine nucleus pulposus cells. Int J Mol Sci **20**: 5036.

Hoffman AS (2012) Hydrogels for biomedical applications. Adv Drug Deliv Rev **64**: 18-23.

Huskisson E, Donnelly S (1999) Hyaluronic acid in the treatment of osteoarthritis of the knee. Rheumatology (Oxford) **38**: 602-607.

Khademhosseini A, Langer R (2007) Microengineered hydrogels for tissue engineering. Biomaterials **28**: 5087-5092.

Kimball JP, Glowczewskie F, Wright TW (2007) Intraosseous blood supply to the distal humerus. J Hand Surg Am **32**: 642-646.

Komorowicz E, Balázs N, Varga Z, Szabó L, Bóta A, Kolev K (2017) Hyaluronic acid decreases the mechanical stability, but increases the lytic resistance of fibrin matrices. Matrix Biol **63**: 55-68.

Laschke MW, Menger MD (2016) Prevascularization in tissue engineering: current concepts and future directions. Biotechnol Adv **34**: 112-121.

Laurens N, Koolwijk Pd, De Maat M (2006) Fibrin structure and wound healing. J Thromb Haemost **4**: 932-939.

LeBoeuf RD, Gregg RR, Weigel PH, Fuller GM (1987) Effects of hyaluronic acid and other glycosaminoglycans on fibrin polymer formation. Biochemistry **26**: 6052-6057.

LeBoeuf RD, Raja R, Fuller G, Weigel P (1986) Human fibrinogen specifically binds hyaluronic acid. J Biol Chem **261**: 12586-12592.

Lee F, Kurisawa M (2013) Formation and stability of interpenetrating polymer network hydrogels consisting of fibrin and hyaluronic acid for tissue engineering. Acta Biomater **9**: 5143-5152.

Levenberg S, Rouwkema J, Macdonald M, Garfein ES, Kohane DS, Darland DC, Marini R, Van Blitterswijk CA, Mulligan RC, D'Amore PA (2005) Engineering vascularized skeletal muscle tissue. Nat Biotechnol **23**: 879-884.

Lin C-H, Wang C-K, Chen Y-A, Peng C-C, Liao W-H, Tung Y-C (2016) Measurement of in-plane elasticity of live cell layers using a pressure sensor embedded microfluidic device. Sci Rep **6**: 36425.

Loebel C, Ayoub A, Galarraga JH, Kossover O, Simaan-Yameen H, Seliktar D, Burdick JA (2019) Tailoring supramolecular guest-host hydrogel viscoelasticity with covalent fibrinogen double networks. J Mater Chem B **7**: 1753-1760.

Lorentz KM, Kontos S, Frey P, Hubbell JA (2011) Engineered aprotinin for improved stability of fibrin biomaterials. Biomaterials **32**: 430-438.

Lu Y-B, Franze K, Seifert G, Steinhäuser C, Kirchhoff F, Wolburg H, Guck J, Janmey P, Wei E-Q, Käs J (2006) Viscoelastic properties of individual glial cells and neurons in the CNS. Proc Natl Acad Sci U S A **103**: 17759-17764.

Maharjan AS, Pilling D, Gomer RH (2011) High and low molecular weight hyaluronic acid differentially regulate human fibrocyte differentiation. PLoS One **6**: e26078. doi: 10.1371/journal.pone.0026078.

McNaught AD, McNaught AD (1997) Compendium of chemical terminology. Blackwell Science [ISBN 0865426848].

Meinhart J, Fussenegger M, Höbling W (1999) Stabilization of fibrin-chondrocyte constructs for cartilage reconstruction. Ann Plast Surg **42**: 673-678.

Montesano R, Kumar S, Orci L, Pepper MS (1996) Synergistic effect of hyaluronan oligosaccharides and vascular endothelial growth factor on angiogenesis *in vitro*. Lab Invest **75**: 249-262.

Morin KT, Tranquillo RT (2013) *In vitro* models of angiogenesis and vasculogenesis in fibrin gel. Exp Cell Res **319**: 2409-2417.

Novosel EC, Kleinhans C, Kluger PJ (2011) Vascularization is the key challenge in tissue engineering. Adv Drug Deliv Rev **63**: 300-311.

Park K-H, Kim H, Moon S, Na K (2009) Bone morphogenic protein-2 (BMP-2) loaded nanoparticles mixed with human mesenchymal stem cell in fibrin hydrogel for bone tissue engineering. J Biosci Bioeng **108**: 530-537.

Park SH, Park SR, Chung SI, Pai KS, Min BH (2005) Tissue-engineered cartilage using fibrin/hyaluronan composite gel and its *in vivo* implantation. Artif Organs **29**: 838-845.

Pelissier P, Villars F, Mathoulin-Pelissier S, Bareille R, Lafage-Proust M-H, Vilamitjana-Amedee J (2003) Influences of vascularization and osteogenic cells on heterotopic bone formation within a madreporic ceramic in rats. Plast Reconstr Surg **111**: 1932-1941.

Raines EW (2000) The extracellular matrix can regulate vascular cell migration, proliferation, and survival: relationships to vascular disease. Int J Exp Pathol **81**: 173-182.

Richards HJ (1980) Repair and healing of the divided digital flexor tendon. Injury **12**: 1-12.

Rico F, Roca-Cusachs P, Gavara N, Farré R, Rotger M, Navajas D (2005) Probing mechanical properties of living cells by atomic force microscopy with blunted pyramidal cantilever tips. Phys Rev E Stat Nonlin Soft Matter Phys **72**: 021914. doi: 10.1103/PhysRevE.72.021914.

Rollwagen F, Pacheco N, Baqar S (1993) An improved model for the examination of biological effects of locally administered cytokines. J Immunol Methods **166**: 223-232.

Rooney P, Kumar S, Ponting J, Wang M (1995) The role of hyaluronan in tumour neovascularization. Int J Cancer **60**: 632-636.

Rooney P, Wang M, Kumar P, Kumar S (1993) Angiogenic oligosaccharides of hyaluronan enhance the production of collagens by endothelial cells. J Cell Sci 1**05**: 213-218.

Rowe SL, Stegemann JP (2006) Interpenetrating collagen-fibrin composite matrices with varying protein contents and ratios. Biomacromolecules **7**: 2942-2948.

Sahni A, Francis CW (2000) Vascular endothelial growth factor binds to fibrinogen and fibrin and stimulates endothelial cell proliferation. Blood **96**: 3772-3778.

Sahni A, Odrljin T, Francis CW (1998) Binding of basic fibroblast growth factor to fibrinogen and fibrin. J Biol Chem **273**: 7554-7559.

Schenk S, Chiquet-Ehrismann R, Battegay EJ (1999) The fibrinogen globe of tenascin-C promotes basic fibroblast growth factor-induced endothelial cell elongation. Mol Biol Cell **10**: 2933-2943.

Slevin M, Kumar S, Gaffney J (2002) Angiogenic oligosaccharides of hyaluronan induce multiple signaling pathways affecting vascular endothelial

cell mitogenic and wound healing responses. J Biol Chem **277**: 41046-41059.

Snyder TN, Madhavan K, Intrator M, Dregalla RC, Park D (2014) A fibrin/hyaluronic acid hydrogel for the delivery of mesenchymal stem cells and potential for articular cartilage repair. J Biol Eng **8**: 10 doi: 10.1186/1754-1611-8-10.

Spargo B, Rudolph A, Rollwagen F (1994) Recruitment of tissue resident cells to hydrogel composites: *in vivo* response to implant materials. Biomaterials **15**: 853-858.

Syedain ZH, Bjork J, Sando L, Tranquillo RT (2009) Controlled compaction with ruthenium-catalyzed photochemical cross-linking of fibrin-based engineered connective tissue. Biomaterials **30**: 6695-6701.

Tayapongsak P, O'Brien DA, Monteiro CB, Arceo-Diaz LY (1994) Autologous fibrin adhesive in mandibular reconstruction with particulate cancellous bone and marrow. J Oral Maxillofac Surg **52**: 161-165.

Tremblay PL, Hudon V, Berthod F, Germain L, Auger FA (2005) Inosculation of tissue-engineered capillaries with the host's vasculature in a reconstructed skin transplanted on mice. Am J Transplant **5**: 1002-1010.

Tuan T-L, Song A, Chang S, Younai S, Nimni ME (1996) *In vitro* fibroplasia: Matrix contraction, cell growth, and collagen production of fibroblasts cultured in fibrin gels. Exp Cell Res **223**: 127-134.

Vigetti D, Viola M, Karousou E, Rizzi M, Moretto P, Genasetti A, Clerici M, Hascall VC, De Luca G, Passi A (2008) Hyaluronan-CD44-ERK1/2 regulate human aortic smooth muscle cell motility during aging. J Biol Chem **283**: 4448-4458.

Weigel P, Frost S, McGary C, LeBoeuf R (1988) The role of hyaluronic acid in inflammation and wound healing. Int J Tissue React **10**: 355-365.

Weigel PH, Fuller GM, LeBoeuf RD (1986) A model for the role of hyaluronic acid and fibrin in the early events during the inflammatory response and wound healing. J Theor Biol **119**: 219-234.

Weisel J (2007) Structure of fibrin: impact on clot stability. J Thromb Haemost **5 Suppl 1**: 116-124.

Wong C, Inman E, Spaethe R, Helgerson S (2003) Fibrin-based biomaterials to deliver human growth factors. Thromb Haemost **89**: 573-582.

Yu Y, Brouillette MJ, Seol D, Zheng H, Buckwalter JA, Martin JA (2015) Use of recombinant human stromal cell-derived factor 1α-loaded fibrin/hyaluronic acid hydrogel networks to achieve functional repair of full-thickness bovine articular cartilage by homing of chondrogenic progenitor cells. Arthritis Rheumatol **67**: 1274-1285.

Editor's note: There were no questions from reviewers for this paper. The Scientific Editor responsible for this paper was Juerg Gasser.